THE JOURNAL OF PHYSICAL CHEMISTRY B

Article

pubs.acs.org/JPCB

Langevin Dynamics Simulation of 3D Colloidal Crystal Vacancies and Phase Transitions

Rozita Laghaei, Sanford A. Asher, and Rob D. Coalson*

Department of Chemistry, University of Pittsburgh, Pittsburgh, Pennsylvania 15260, United States

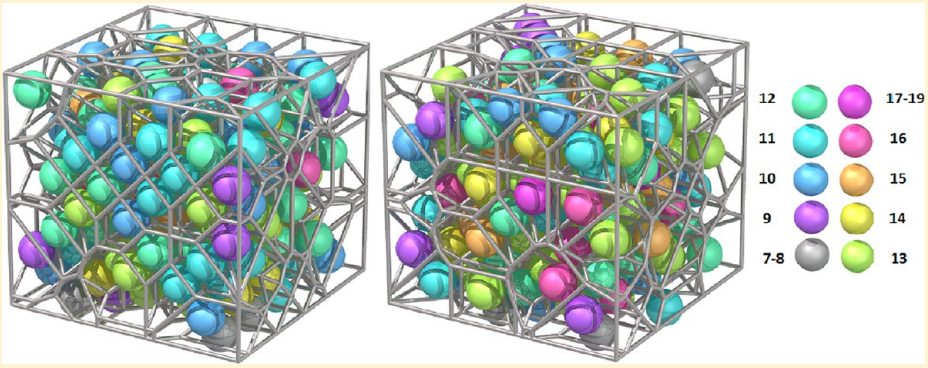

ABSTRACT: We study the mechanism of vacancy migration and phase transitions of 3D crystalline colloidal arrays (CCA) using Langevin dynamics simulations. We calculate the self-diffusion coefficient of the colloid particles and the diffusion constant for vacancies as a function of temperature and DLVO potential parameters. We investigate the phase behavior of several systems with different interaction potential parameters using Voronoi analysis. Voronoi polyhedra tessellation, which is a useful method for characterizing the nearest neighbor environment around each atom, provides an efficient and effective way to identify phase transitions as well as geometrical changes in crystals. Using Voronoi analysis, we show that several neighboring particles are involved in the vacancy migration process that causes the vacancy to diffuse.

INTRODUCTION

Dispersions of colloidal particles provide a useful model for studying the fundamental physics of phenomena such as crystal nucleation and growth, the glass transition,[1,2] and melting phase transitions at experimentally convenient length and time scales.[3,4] Colloidal crystals display phase transitions between FCC, BCC, liquid, and gas phases. Prediction of the phases that are stable for different electrostatic interaction parameters may help in understanding the mechanisms and dynamics of nucleation and melting and thus in controlling the equilibrium structures of the system.

In this paper, we study crystalline colloidal arrays (CCAs), highly ordered arrays of like-charged colloidal particles typically self-organized into an FCC lattice. Among the most widely experimentally studied CCAs are those comprised of monodisperse negatively charged polystyrene spheres.[5−8] The complete CCA system consists of charged colloidal particles (macroions), their counterions, salt ions, and solvent molecules. The interactions between the charged macroions are modeled via an effective DLVO pair potential. In DLVO theory (introduced by Derjaguin and Landau[9] and Verwey and Overbeek[10]), the Coulombic repulsion between two macroions is screened exponentially by the surrounding electrolyte ions such that it gives rise to a Yukawa-like interaction:

$$U_{\mathrm{DLVO}}(r) = W\frac{\exp(-\kappa(r-\sigma))}{r} \tag{1}$$

where r is the distance between the centers of the two colloid particles, σ is the colloid diameter, κ is the inverse Debye screening length (which depends upon the ionic strength of the solution), and

$$W = \frac{Z^{*2}e^2}{4\pi\varepsilon\varepsilon_0(1+\kappa\sigma/2)^2} \tag{2}$$

Here Z^* is the effective charge on each colloid particle in units of the elementary charge e, ε is the static dielectric constant of water which is 78 at 300 K, and ε_0 is the vacuum permittivity. For a solution containing concentrations n_j of z_j-valent ions,

$$\kappa^2 = 4\pi\lambda_{\mathrm{B}}\sum_{j=1}^{m} n_j z_j^{\,2} \tag{3}$$

where m is the number of ionic species and $\lambda_{\mathrm{B}} = e^2/(4\pi\varepsilon\varepsilon_0 k_{\mathrm{B}}T)$ is the Bjerrum length at absolute temperature T (k_{B} being Boltzmann's constant). In a colloidal suspension with highly charged colloid particles, the liquid layer surrounding each colloid particle can be subdivided into an inner layer, termed the Stern layer, where the counterions (with opposite charge to the colloid charge) are strongly bound, and an outer layer,

Received: September 20, 2012
Revised: January 28, 2013

   dx.doi.org/10.1021/jp309363h | J. Phys. Chem. B XXXX, XXX, XXX−XXX

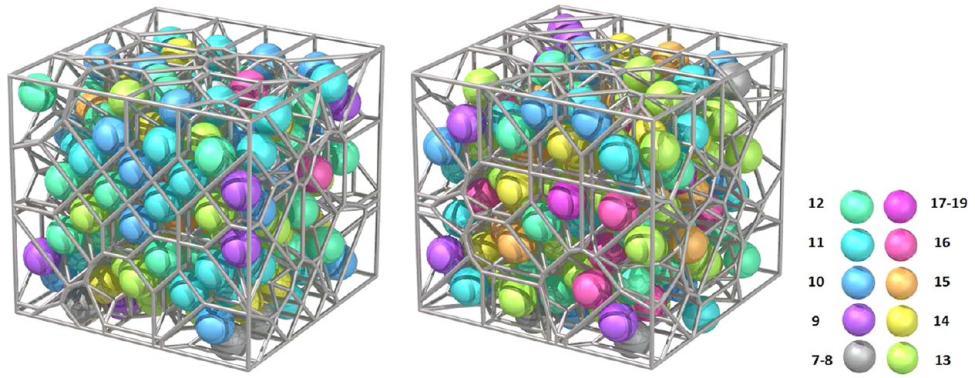

Figure 1. Three-dimensional computation of Voronoi cells. The number of faces associated with a given cell is indicated by the color of the central particle (see right panel). The boxes are ~10% of our simulation box (containing 256 particles) at different simulation times: the left box is close to the start of the simulation, and the right box is a snapshot several time steps into the simulation. (Note: For plotting purposes, the ratio of particle diameter to the unit cell length shown here has been set to be roughly 2 times larger than the actual ratio.) This figure was plotted using a Perl script provided by ref 24.

where the counterion association is weak (often referred to as the "diffuse layer"). The thickness of the double layer depends on the concentration of ions in solution. When the colloid charge is very high, the counterions in the Stern layer reduce the bare colloid charge to an effective charge, Z^*. The effective (or renormalized) charge and Debye length can be estimated by numerically solving the nonlinear Poisson−Boltzmann equation.[11−14] Note that it is also useful to define the value of the potential energy when the spheres are in contact[15]

$$\beta\varepsilon = \frac{Z^{*2}}{(1 + \kappa\sigma/2)^2}\frac{\lambda_B}{\sigma} \tag{4}$$

where $\beta = 1/k_BT$ is the inverse temperature. All other system parameters being fixed, this contact potential is a surrogate for Z^*.

Three-dimensional CCAs have often been used as model systems for interparticle interactions in solution.[16−18] However, little is known about the properties of vacancies that may develop in a perfect CCA. Theoretical methods such as molecular dynamics, Langevin dynamics, and Monte Carlo simulations can help to shed light on these details.

The Langevin dynamics technique is a method for simulating the dynamics of particles in a dissipative environment at finite temperature. The Langevin equation is a stochastic differential equation in which two additional forces, a frictional damping force and a random force, are added to Newton's second law. The friction term approximates collisional effects of solvent molecules that are not explicitly present in the system. The random force is associated with the thermal motions of the solvent molecules. Langevin dynamics provides a way to coarse grain the fast modes that characterize the solvent, thus allowing us to simulate longer time scales than would a molecular dynamics simulation in which solvent molecules were explicitly included.

In the first part of this paper, we use Langevin simulations to investigate the mechanism of vacancy migration in three-dimensional crystalline colloidal arrays whose particles interact through a DLVO pair potential.[9,10] In particular, we calculate the diffusion coefficient of a single vacancy. In the second part of the paper, we investigate the melting transition of the colloidal crystals of the type used in our recent experiments (S. Asher[5−8]) by varying the DLVO potential parameters.

METHODS

Langevin Simulations. We utilized the stochastic Langevin equation integrator proposed by Bussi and Parinello in ref 19 to sample canonical ensemble equilibrium in our systems. Here a dissipative force and noise are added to the Hamilton equations of motion to model the dynamics of the massive particles in their bath of (small) solvent particles. The Langevin equations of motion for a particular Cartesian degree of freedom (x, y, z) of a particular particle are

$$dp(t) = -\frac{\partial U}{\partial q}dt - \gamma p(t)dt + \sqrt{\frac{2m\gamma}{\beta}}\eta(t)dt \tag{5}$$

$$dq(t) = \frac{p(t)}{m}dt \tag{6}$$

where $U(\vec{q})$ is the system potential energy and depends on all system coordinates $\vec{q}$, m is the particle mass, γ is the friction coefficient, p is the momentum, and q is the relevant position component of the particle under consideration. Furthermore, $\eta(t)$ is a Gaussian white noise time series with zero time average, $\langle\eta(t)\rangle = 0$, and obeying

$$\langle\eta(t)\eta(t')\rangle = \delta(t - t') \tag{7}$$

The first term on the r.h.s. of eq 5 is the deterministic force. The multiple time step integrator developed in ref 19 was shown there to be accurate even in the high friction limit. Hydrodynamic interactions were neglected in our simulations.

Simulation Details. We began by studying a system of 499 particles in an FCC lattice with one vacancy and packing fractions (the ratio of volume that is occupied by particles in the unit cell to the volume of the unit cell) of 0.74, 0.6, and 0.22 to determine the mechanism of vacancy migration in three dimensions. The particle diameter was 1000 Å. The system became equilibrated after 10^6 to 5×10^6 time steps and the last 5×10^6 structures were analyzed. We used simulation times of 10^7 to 4×10^7 time steps of 5 fs at temperatures between 100 and 300 K. The Langevin friction constant chosen was 0.01 (time step)$^{-1}$, the pair potential cutoff distance was 2.5σ (close to half of the box length), $\kappa = 5/\sigma$ (Å^{-1}), and W = 850.0 to $1500 \times 0.59227 \times \sigma/298.0$ ([kcal/mol]Å).

We subsequently investigated the dependence of the phase transition behavior of a defect-free CCA of 2048 particles on the interaction potential. This simulation system was

dx.doi.org/10.1021/jp309363h | J. Phys. Chem. B XXXX, XXX, XXX−XXX

characterized by the following conditions: periodic boundary conditions were applied, and an FCC lattice was constructed with packing fractions of 0.05 and 0.1. The colloid diameter was chosen to be 1000 Å at 300 K, and the Langevin friction constant was set to 0.1 (time step)$^{-1}$. Furthermore, the cutoff distance for pairwise interactions was taken to be 8.0σ (corresponding to a pair interaction strength of 10^{-9} k_BT); $\kappa\sigma$ ranged between 0.6 and 12, and Z^* varied between 200 and 600, with the simulation time being 2×10^7 time steps.

Voronoi Analysis. The structures of these colloidal systems were analyzed using the Voronoi diagram, a widely employed tessellation method. The Voronoi diagram provides a way to partition space. Each particle of the system is associated with a single Voronoi cell. The Voronoi diagram of a set of particles partitions the space into convex cells, in such a way that all points within a Voronoi cell are nearer to the central particle than any other particle. In chemistry and materials science, the first studies that utilized the Voronoi analysis were by John Bernal who studied the structure of molecular systems. Bernal suggested that "many of the properties of liquids can be most readily appreciated in terms of the packing of irregular polyhedra".[20] Another application of Voronoi tessellation is in crystallography,[21,22] where it has been applied to calculate atomic volumes in crystallographic structures of ribonuclease C and lysozyme.[23]

The Voronoi method is also very useful for the analysis of a system comprised of a number of separate sites (occupied by ions, molecules, ...), by dividing the space between the particles according to their nearest neighbors, since the properties of the system depend on the positions of the particles and their spatial distribution. An FCC lattice gives a rhombic dodecahedra tessellation of space, while a BCC lattice gives truncated octahedra. For an illustrative system and its Voronoi cells, see Figure 1. To plot this figure, ~10% of the simulation box of one of our CCA systems, with packing fraction = 5%, Z^* = 425, and $\kappa\sigma$ = 3.3, was used and a Perl script provided in refs 24 and 25 was employed.

In our system, the time evolution of a vacancy created by removing one particle located at the center of the simulation box from the periodic lattice at time t = 0 was tracked using Voronoi analysis. At each time step, we monitored the number of nearest neighbors surrounding each colloidal particle. We computed the number of edges, the number of faces, and the total surface area of the Voronoi cells. Furthermore, for each cell, we monitored the cell centroid, the cell volume, and the number of neighboring particles that created each face of the cell. As discussed below, we found that vacancy migration involves several neighboring particles which are dislocated (i.e., not positioned at crystal lattice sites) during the diffusion of the vacancy. By tracking the Voronoi cells and their properties (number of faces and volumes), we were able to extract the trajectory of the vacancy, and gain insight into the mechanism of vacancy migration and the role of neighboring particles in vacancy diffusion. The Voronoi analysis was performed using the *voro++*[24] code, version 0.3.1.

In this work, we use the Voronoi cell volumes to determine the positions of the vacancies. The vacancy volume is shared by neighboring particles. Therefore, by averaging the particle positions with the largest Voronoi volume (eq 8), we can calculate the location of the vacancy centers, $\mathbf{r}_v$, and follow the vacancy diffusion. Specifically, we compute

$$\mathbf{r}_v = \frac{1}{N}\sum_{i=1}^{N} \mathbf{r}_i \tag{8}$$

Here the integer i indicates the ordering of the Voronoi volumes (i = 1 labels the largest volume, with $\mathbf{r}_i$ being the position of the centroid of the ith Voronoi volume) and N is the number of particles with Voronoi volumes significantly larger than that of the bulk. Typically, we utilized $N \leq 6$. The average for each particle can be calculated by subtracting the Voronoi volume of a particle from 1/4 of the FCC lattice unit cell volume. For 2D systems,[26] the vacancy configuration is usually identified according to the number of sides of the polygons in the Voronoi construction. For an ideal 2D hexagonal system, all particles have a coordination number (number of nearest neighbors) of six. In the presence of vacancies, the coordination number of the neighboring particles will differ from six. The vacancy is localized at the center of particles with coordination number $z_i \neq 6$. However, our 3D system is more topologically complex than its 2D analogue, and hence the coordination number (in 3D the number of Voronoi faces) does not provide a convenient measure of the vacancy position and the participation of neighboring colloidal particles in the vacancy migration. In an ideal FCC system, the number of nearest neighbors for each particle is 12. It is rather complicated to track the particles with $z_i \neq 12$ and find their geometric center. A more effective procedure is to follow the particles with the highest Voronoi volume.

RESULTS AND DISCUSSION CONCERNING VACANCY MIGRATION

Vacancy Migration in a Colloidal Crystal Array. The vacancies pass through various distinct configurations between lattice sites due to thermal fluctuations, as illustrated in Figures 2 and 3, which treat a system having a packing fraction of 10%

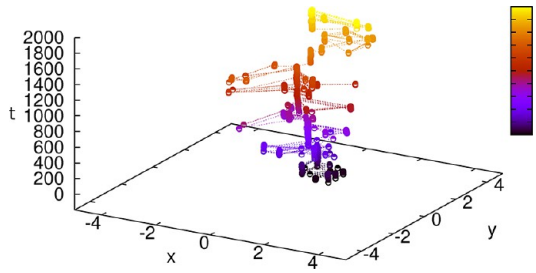

Figure 2. A typical trajectory of the vacancy. The 3D trajectory is projected onto the x–y plane, and the simulation time is encoded with color along the t axis. The system is in a crystal phase with packing fraction 10%, Z^* = 510, and $\kappa\sigma$ = 5. We analyzed the system configurations and calculated the vacancy position every 5000 time steps.

with Z^* = 510 and $\kappa\sigma$ = 5. For a system of 499 particles, we analyzed the system configurations and calculated the vacancy positions every 5000 time steps. In Figure 2, a three-dimensional trajectory is projected in the x–y plane and the simulation time is encoded with color along the t axis, while, in Figure 3, the same trajectory is projected onto a two-dimensional plane. It is clear particularly from Figure 3 that the vacancy typically hops from a crystal lattice site to the midpoint between two lattice sites; then it hops backward or forward to a lattice site. Thus, the midpoint position between lattice sites appears to be a metastable minimum in the effective

dx.doi.org/10.1021/jp309363h | J. Phys. Chem. B XXXX, XXX, XXX–XXX

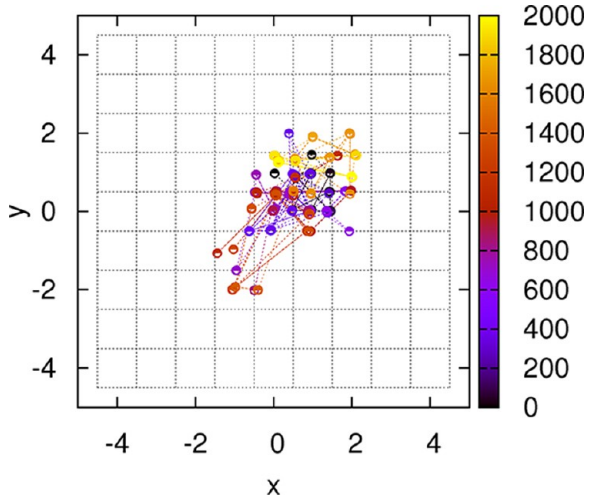

Figure 3. A typical trajectory of the vacancy. The system properties are the same as Figure 2. The same 3D trajectory shown in Figure 2 is projected here in the $x-y$ plane in 2D. Nodes along the dashed lines indicate crystal lattice sites. (Recall that this 2D plane represents a projection from 3D, so the indicated lattice positions here represent FCC lattice sites that occur at different z values in 3D.)

potential energy surface that governs the motion of a vacancy. Direct hops of the vacancy from one lattice site location to an adjacent lattice site are not observed in our simulations, indicating that they occur only rarely or not all. Again, this points to the existence of accessible midpoint states lying between crystal lattice site positions.

For a system initially comprised of a single vacancy, we observe that a split-vacancy configuration (SV), i.e., two vacancy regions separated by a dislocated particle, is stable, and indeed is the configuration most frequently seen in the simulations. At the beginning of the simulations, all particles reside at their FCC site positions and the initial vacancy volume is shared by all 12 nearest neighbors. After the simulation starts, these neighboring particles move toward the vacant site to lower the total potential energy of the system. We often see that one particle moves to the midpoint between its lattice site and the initial vacancy lattice site. In this case, the Voronoi cell volume that belongs to this particle increases (Figure 4). We find that there are typically one to three neighboring particles around the vacancy that have the highest Voronoi volumes (the particles that moved toward the vacancy), whereas the rest of the neighboring particles have Voronoi volumes close to that of the normally packed bulk particle Voronoi volume.

Figure 4 shows the changes in the values of the first and second highest Voronoi volumes of particles that are nearest neighbors to the initial vacancy, as a function of the simulation time. At the beginning of the simulation, Voronoi analysis shows that the vacancy volume is equally divided among the 12 nearest neighbors. During the course of the simulation, the neighboring particle/particles move toward the vacancy; the vacancy volume is now divided among the particles that are closest to the vacancy center. When the difference between the two highest Voronoi volumes of the nearest neighbors is large, it means that one particle has moved toward the vacancy and the Voronoi cell containing that particle has the highest volume. Therefore, the difference between the highest volume and the second highest volume increases. This configuration is the so-called split vacancy configuration. Similarly, Figure 5 shows the largest and second largest number of faces as a

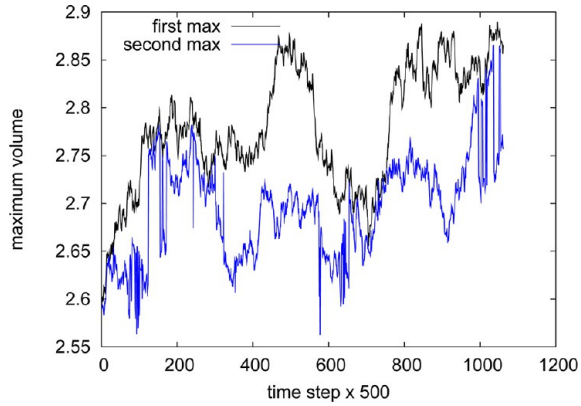

Figure 4. Comparison of the first and second largest Voronoi volumes for a 499 particle CCA having packing fraction = 0.219 with W = 1500 at T = 100 K, measured every 500 time steps. When the difference between the first and second highest Voronoi volumes is large, i.e., at time ~450−550 (time step × 500) and 750−950, only one particle is significantly displaced toward the vacancy center (split vacancy configuration), while at times ~150−250, 650−750, and 1000, two or more particles are displaced to fill the vacancy.

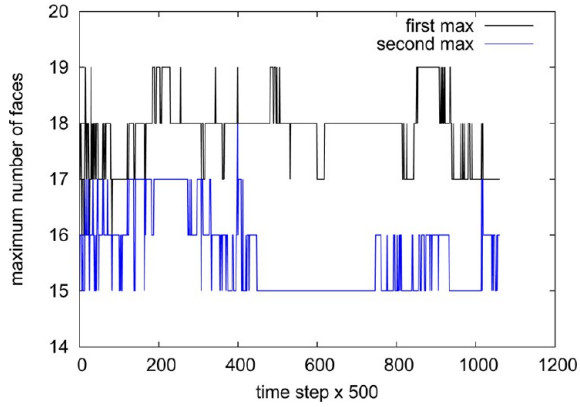

Figure 5. Comparison of the first and second maximum number of faces in Voronoi polygons for a system with packing fraction = 0.219 at T = 100 K, measured every 500 time steps. See the Figure 4 caption for further details.

function of the simulation time. We see here that the Voronoi volume is a more informative measure than the number of Voronoi faces because the Voronoi volume is a continuous variable and follows the time evolution in a simpler manner.

The FCC crystal with a single vacancy appears to be in a stable, equilibrium state; i.e., the vacancy remains present throughout the simulation. This stands in contrast to systems consisting of hard cubes with extremely high equilibrium vacancy concentration.[27−29] In such systems, new vacancies can appear spontaneously, as the system can lower its free energy by forming vacancies.

Particle Self-Diffusion. Colloid particle self-diffusion coefficients were calculated at various temperatures in longer simulations (4×10^7 time steps) by employing the Einstein relation, which relates the diffusion coefficient to the mean square displacement of the particles. The appropriate relationship for a 3D system is

$$D = \lim_{t\to\infty} \frac{1}{6N_m t} \left\langle \sum_{j=1}^{N_m} [\mathbf{r}_j(t) - \mathbf{r}_j(0)]^2 \right\rangle \quad (9)$$

dx.doi.org/10.1021/jp309363h | J. Phys. Chem. B XXXX, XXX, XXX−XXX

where N_m is the number of colloid particles, t is the time, and $(\mathbf{r}_j(t) - \mathbf{r}_j(0))$ is the vector distance traveled by particle j over the time interval. The term $(1/N_m)\langle\sum_{j=1}^{N_m}[\mathbf{r}_j(t) - \mathbf{r}_j(0)]^2\rangle$ is the mean square displacement averaged over the total number of particles N_m. The angled brackets in eq 9 indicate an ensemble average, which we implement here by averaging over all possible time origins. We calculated the self-diffusion coefficient for the system having a packing fraction of 0.74, with $\kappa = 5/\sigma$ (Å^{-1}) and $W = 1678$ ([kcal/mol]Å) at different temperatures from 100 to 300 K ($\beta\varepsilon$ from 2.83 to 8.5). Figure 6, upper panel, shows that the colloid particle self-diffusion coefficient increases nearly linearly with temperature.

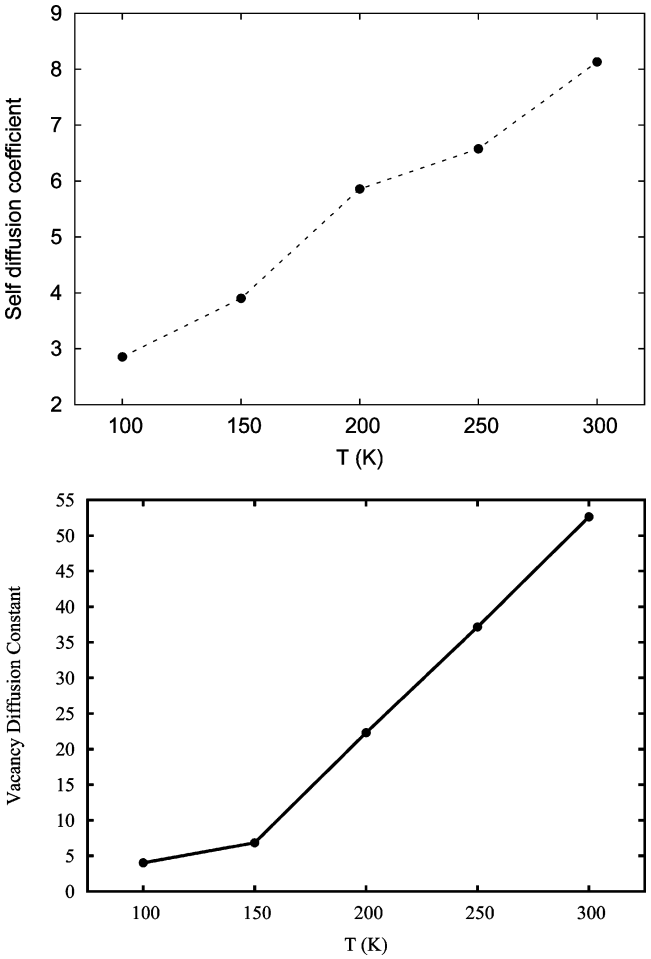

Figure 6. Upper: Temperature dependence of colloid particle self-diffusion coefficient ($\times 10^{-5}$ cm^2/s). The simulation time was 4×10^7 time steps, each time step being 5 fs. Lower: Vacancy diffusion constant as a function of temperature. The diffusion constant is given in units of ($\times 10^{-5}$ cm^2/s). These diffusion constants pertain to the motion of the vacancy center, computed as discussed in the text.

Vacancy Diffusion Constant. The position of the vacancy is either very close to a lattice site or between two lattice sites, the latter case corresponding to what we call a split-vacancy configuration (SV). Increased temperature results in faster motion of the vacancy. Vacancy diffusion proceeds primarily along the major CCA symmetry axes, in agreement with previous 2D simulation results (see Figure 3 of ref 26). We observed that the vacancy diffusion constant is nearly the same (isotropic) in all three Cartesian dimensions.

We calculated the temperature dependence of the vacancy diffusion constant for the system with a packing fraction of 0.74 and $\kappa = 5/\sigma$ (Å^{-1}) and $W = 1678$ ([kcal/mol]Å). Analogously to eq 9 above,

$$D_v = \frac{1}{6}\lim_{t\to\infty}\frac{\langle[\mathbf{r}_v(t) - \mathbf{r}_v(0)]^2\rangle}{t} \tag{10}$$

where $\mathbf{r}_v$ is the vacancy center position computed from eq 8. To implement eq 10, we ran one long trajectory (out to $t = 4 \times 10^7$ time steps), and then used linear regression to extract the value of D. The diffusion constant increases roughly linearly with temperature (Figure 6, lower panel), in agreement with the analogous 2D system studied by Libal et al.[26] (see Figure 8 of ref 26). Comparison of the particle diffusion coefficients (Figure 6, upper panel) with the vacancy diffusion constant (Figure 6, lower panel) indicates a larger diffusion for the vacancies, especially at higher temperatures.

As explained earlier, vacancy displacement occurs via a complex mechanism which involves several neighboring particles. As described above, the location of the vacancy is determined by averaging the positions of the few particles ($N \leq 6$, and often $N = 1-3$) that have unusually high Voronoi volumes. These particles, being surrounded by a relatively large amount of free volume, are relatively mobile, leading to a relatively high vacancy diffusion constant. In contrast, the remaining particles in the lattice, which are not in the immediate vicinity of the vacancy region, are relatively immobile. The particle diffusion constant values reported in Figure 6 (upper panel) are obtained by averaging the diffusion constants calculated for all particles in the system. By virtue of this definition, the net particle diffusion constant is reduced relative to the corresponding vacancy diffusion constant at the same temperature.

PHASE TRANSITION

In the second part of the present study, we examined the dependence of the phase behavior of defect-free FCC colloidal crystals of 2048 particles at 300 K, as we varied the effective colloid particle charge and the inverse Debye screening lengths guided by the Poisson–Boltzmann cell model of Alexander et al.[14] Voronoi analysis proved to be useful in these endeavors.

Average Number of Voronoi Polygon Faces. The distribution of the number of Voronoi polygon faces was calculated for all colloidal particles and averaged over the total simulation time. This distribution provides a convenient measure of the deviation of the particle positions from their original crystal site locations.

When the system is in a perfect FCC crystal, the distribution is sharp, while in the liquid phase it is broad. The distribution of the number of Voronoi polygon faces is shown in Figure 7, focusing on the effects of Z^*, the effective colloidal charge, upon the stability of an FCC crystal. Upon increasing Z^* from 200 to 600 at constant $\kappa\sigma = 5$ (corresponding to a 20 nm Debye length) and packing fraction 0.1, the distribution of the number of Voronoi polygon faces sharpens (note that the Z^* values 200, 250, 300, 380, 450, 510, and 600 at 300 K and $\kappa\sigma = 5$ correspond to $\beta\varepsilon = 46.35$, 72.43, 104.3, 167.34, 234.68, 301.43, and 417, respectively). The maximum probability occurs at a value close to 14 faces, instead of the value of 12 expected for an FCC lattice, due to the topological instability that results from thermal fluctuation. When particles execute thermal fluctuations about their equilibrium lattice sites, the

dx.doi.org/10.1021/jp309363h | J. Phys. Chem. B XXXX, XXX, XXX–XXX

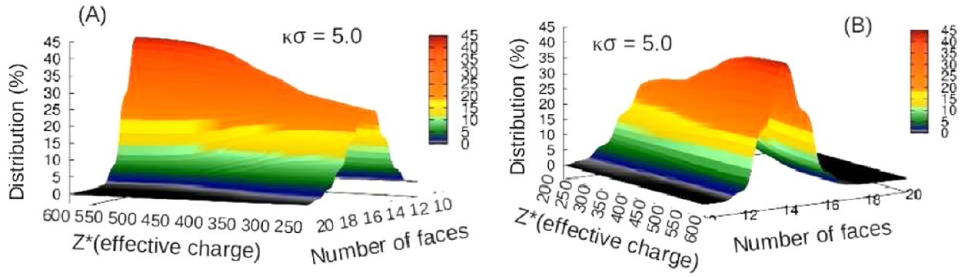

Figure 7. The percent distribution (%) of the number of Voronoi faces averaged over the simulation time when $\kappa\sigma = 5$ (corresponding to a Debye length = $1/\kappa$ = 20 nm) and packing fraction = 0.1, shown from two different viewing angles in panels A and B.

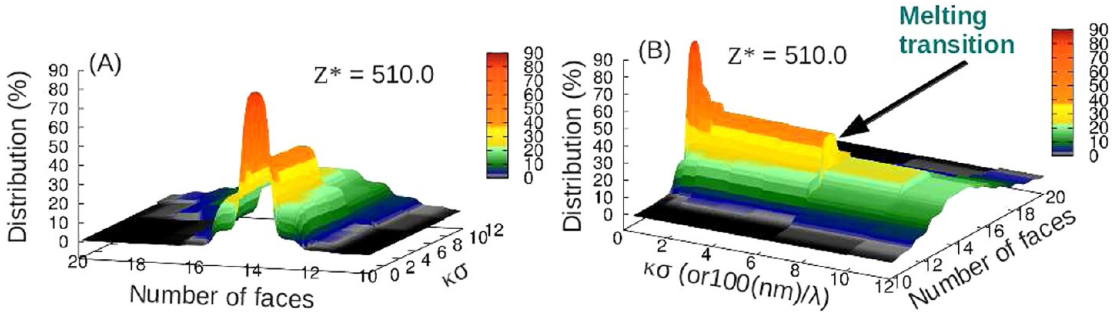

Figure 8. The distribution (%) of the number of Voronoi faces for Z^* (effective charge) = 510, shown from two different viewing angles in panels A and B.

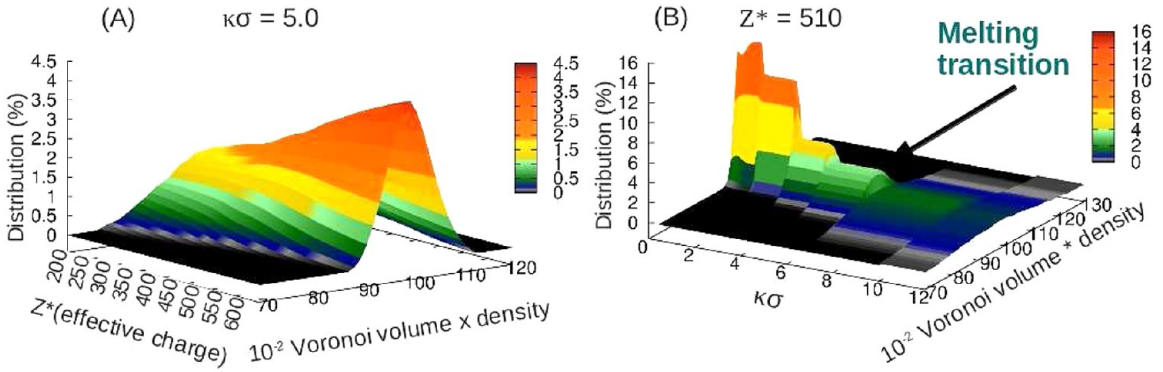

Figure 9. (A) Surface plot of the distribution (%) of Voronoi volumes in 3D (divided by (V/N) where V is the volume of the simulation box and N is the number of particles) averaged over the simulation time for $\kappa\sigma = 5.0$. (B) Distribution of Voronoi volumes averaged over the simulation time for $Z^* = 510$. The packing fraction is 0.1.

number of particles which share a small face is spuriously increased and therefore the number of particles identified as nearest neighbors is increased.

Theoretical as well as numerical simulations studies for Lennard-Jones, hard spheres, and hard disks[30−32] show that slight perturbations of position transform a vertex of a Voronoi polyhedron into a Voronoi surface. As a result, polyhedra with 12−18 faces coexist in our system, with a mean value at 14.[30−32] The distribution of Voronoi polygon faces changes dramatically with Debye length at constant $Z^* = 510$ and packing fraction = 0.1; cf. Figure 8. The broadening of the distribution results from the melting of the FCC lattice, as is clearly evident in Figure 8B.

Average Voronoi Polygon Volumes. Figure 9 shows a three-dimensional surface plot of the distribution of the Voronoi polygon volumes, while Figure 10 shows a two-dimensional contour plot representation of the same quantity. The CCA melting transition can be monitored via changes in the distribution of the number of Voronoi polygon faces or the distribution of Voronoi volumes. The Voronoi volume dependence, which can be calculated as a function of Z^* or $\kappa\sigma$, shows similar properties as the Voronoi polygon face dependence. As Z^* decreases from 600 to 200 at a constant Debye length, the FCC crystal melts, resulting in a broadened distribution for $Z^* < 380$ (Figure 9A). Just as was found with the distribution of the number of Voronoi faces, changes in Debye length also have a strong effect on the distribution of Voronoi volumes; cf. Figure 9B. Both measures (Voronoi face number distribution and volume distribution) indicate that the melting transition occurs when $\kappa\sigma$ is ∼6.

In a previous study on Voronoi polyhedra volume distributions[31] for a system characterized by a Lennard-Jones 12-6 pair potential, the normalized volume distribution was found to be rather sharp and nearly symmetric for the crystalline CCA. In the melted state, this distribution was broader and the reduced volumes were less symmetric (ranging from 0.55 to 1.85), but the maximum occurred at the same volume as for the solid. The gas phase was characterized by a

dx.doi.org/10.1021/jp309363h | J. Phys. Chem. B XXXX, XXX, XXX−XXX

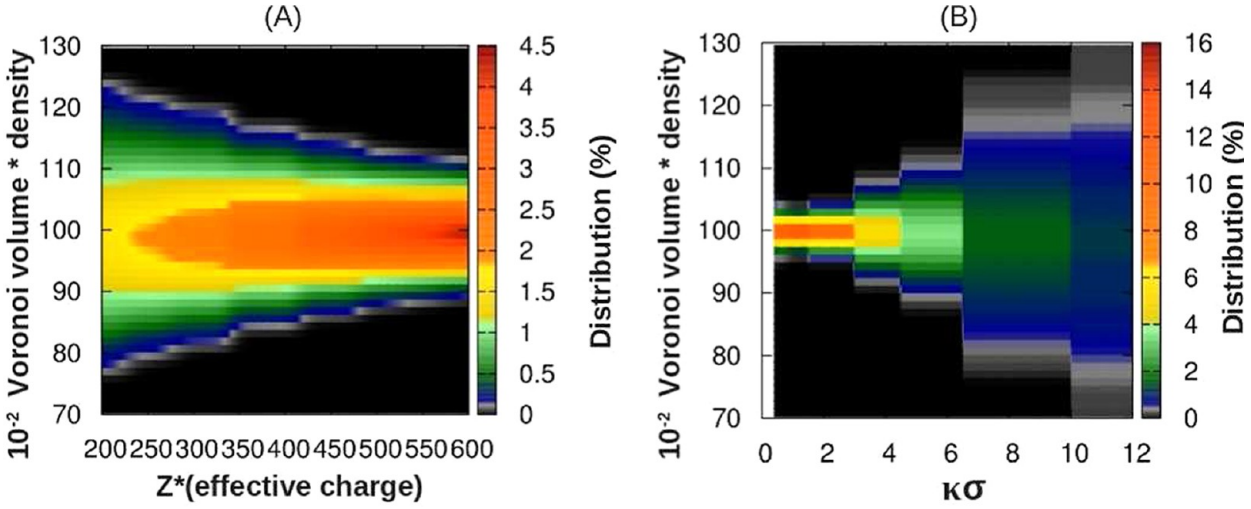

Figure 10. Contour plot of the information depicted in Figure 9. Distribution (%) of Voronoi polygon volumes in 2D (divided by (V/N)) (A) at constant $\kappa\sigma$ = 5 and packing fraction = 0.1 and (B) at constant Z^* = 510 and packing fraction = 0.1.

very wide, almost flat Voronoi volume distribution.[31] Our results show similar behavior for the distribution of the Voronoi volumes in the FCC and liquid phases. For both the volume and the face number distributions, we observe large differences in the distribution widths for $\kappa\sigma > 6$ and $Z^* = 510$. For $Z^* < 380$ and $\kappa\sigma = 5.0$, the system starts to lose its FCC lattice structure. This is seen clearly in Figure 10, which shows 2-D contour plots of the distribution of Voronoi volumes at constant $\kappa\sigma = 5.0$ (A) and at constant $Z^* = 510$ (B).

In ref 15, the phase diagram of colloidal particles with a mesoscopic diameter (i.e., including the effects of a hard core) was studied, and in ref 33 the phase diagram of a point Yukawa system was investigated. Our colloidal system can be considered as a point Yukawa system in the low packing fraction or highly charged colloid limit, while in the low charge or high density limit a hard-core repulsion between colloid particles should be included. In ref 15, the phase behavior of hard core Yukawa particles has been systematically studied. The authors concluded that the phase diagram of hard core repulsive Yukawa particles for contact potential values sufficiently higher than $\beta\varepsilon = 20$ can be calculated from the phase boundaries of the point Yukawa system. They calculated the phase diagram for four contact values, $\beta\varepsilon$ = 8, 20, 39, and 81 (see Figure 5 in ref 15).

Our colloid system falls in the low packing fraction, high charge regime. We can compare some of our results to theirs; namely, the values of Z^* = 200, 250 and $\kappa\sigma = 5$ in our system correspond to $\beta\varepsilon$ = 46.35, 72.43, respectively. We find that the phase behavior of these two $(\beta\varepsilon)$ data points corresponds to a melted state, in agreement with ref 15. The rest of our data points (Figures 9A and 10A for $Z^* > 250$ at constant $\kappa\sigma = 5$ and Figures 9B and 10B for $1 < \kappa\sigma < 12$ at constant $Z^* = 510$) correspond to higher $\beta\varepsilon$ values and thus cannot be compared to results obtained in ref 15. However, they can be compared to the point particle Yukawa phase behavior reported in ref 33: after appropriate unit conversion, all of our data occur in the phase predicted in the Yukawa model (cf. Figure 5 in ref 33).

Lindemann proposed[34] that crystals melt when the root-mean-square displacement of the lattice vibration is relatively high (ca. 10%) compared to the nearest neighbor distance. Calculation of the ratio of the average amplitude of thermal vibrations to the nearest neighbor distances (i.e., $L/\sqrt{2}$ for an FCC lattice, where L is the cell size) of the colloid particles in the CCA at different effective charges (Z^*) and inverse Debye lengths shows that the melting point we calculated using the Voronoi distribution of the number of Voronoi polygon faces and volumes is in very good agreement with the Lindemann criterion; cf. Figure 11 for fixed $\kappa\sigma = 5$ and packing fraction = 0.1, the same system considered in Figure 10A.

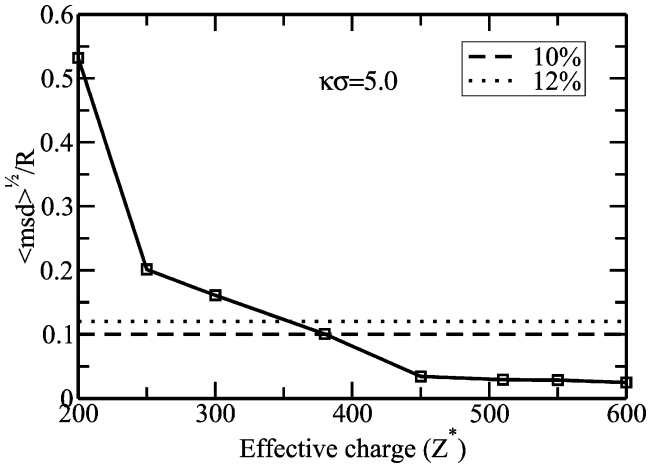

Figure 11. The ratio of the root-mean-square displacement to $R = L/\sqrt{2}$ (ref 35), where L is the cell size as a function of Z^*. The system parameters are the same in Figures 7 and 9A. Melting occurs when the root-mean-square displacement increases above 10−12% of R, indicated by dotted and dashed lines. The bracketed range of the effective charge at which the melting transition occurs is consistent with results obtained via Voronoi analysis, as described in the text.

Self-Diffusion Coefficient. Figures 12 and 13 show the colloid particle self-diffusion coefficients of the systems studied calculated over 2×10^7 time steps. The diffusion coefficient decreases upon either increasing the effective charge or decreasing $\kappa\sigma$.

SUMMARY

In the first part of this paper, we studied via Langevin dynamics the migration of a vacancy in a 3D colloid crystal array (CCA) configured in an FCC lattice, assuming that all pairs of colloid

dx.doi.org/10.1021/jp309363h | J. Phys. Chem. B XXXX, XXX, XXX−XXX

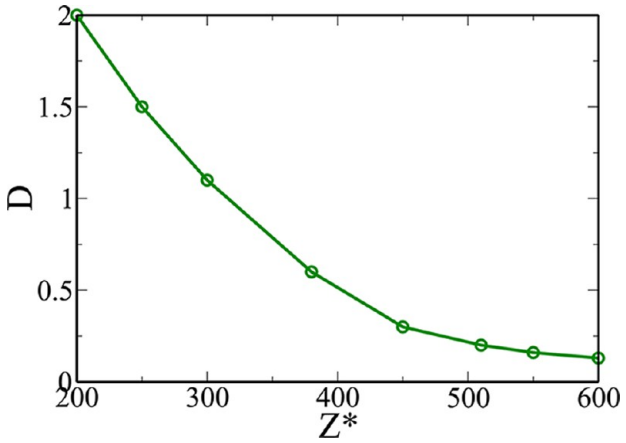

Figure 12. Colloid particle self-diffusion coefficient ($\times 10^{-4}$ cm^2/s) as a function of Z^* at constant $\kappa\sigma$ = 5 and packing fraction = 0.1.

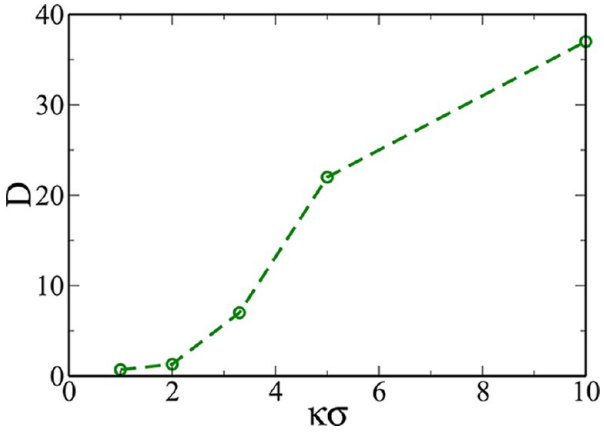

Figure 13. Colloid particle self-diffusion coefficient ($\times 10^{-5}$ cm^2/s) as a function of $\kappa\sigma$ when Z^* = 425 and packing fraction = 0.05.

particles interact via a DLVO potential. The time evolution of the vacancy was tracked using Voronoi analysis. The number of nearest neighbors and the volume of each Voronoi cell were calculated for each colloidal particle. We calculated both the self-diffusion coefficient of the colloid particles and the diffusion constant of the vacancy as a function of temperature.

We found that during the vacancy migration process several neighboring particles dislocate and cause the vacancy to diffuse, without simply hopping in a manner where the neighboring particles remain frozen in their original position while only one particle hops into the vacant position.

We observed that the vacancy is positioned either close to a lattice site or between two lattice sites. The latter configuration is in fact the most often seen in the simulations, consistent with experimental results previously obtained for analogous 2D systems.[26] We also observe dislocation of three or more colloid particles, even at lower temperatures and far from the crystal's melting point.

In the second part of the paper, we examined the phase behavior of a perfect (defect free) CCA at different packing fractions with different effective particle charges and Debye lengths. For a system with a fixed effective colloid charge, we observe FCC crystal melting at larger values of $\kappa\sigma$. Melting of the FCC also occurs at a constant Debye length as the effective particle charge decreases. We also calculated the colloid particle self-diffusion coefficient as a function of the interaction potential. At a constant Debye length, the self-diffusion coefficient increases upon decreasing the effective colloid charge. As expected from the behavior of a system which shows a phase transition from crystal phase to liquid phase, upon increasing the inverse Debye screening length, $\kappa\sigma$, the diffusion coefficient also increases rapidly. The work reported here establishes a foundation for future examination of the behavior of two or more vacancies in a CCA, and thus, ultimately, for understanding both mechanisms and rates of nucleation phenomena in these systems.

AUTHOR INFORMATION

Corresponding Author

*E-mail: coalson@pitt.edu.

Notes

The authors declare no competing financial interest.

ACKNOWLEDGMENTS

This work was supported in part by NSF Grant No. CHE-0848265. Computations presented here were carried out at the University of Pittsburgh's Center for Molecular and Materials Science.

REFERENCES

(1) Pusey, P.; Zaccarelli, E.; Valeriani, C.; Sanz, E.; Poon, W.; Cates, M. Hard Spheres: Crystallization and Glass Formation. *Philos. Trans. R. Soc., A* **2009**, *367*, 4993−5011.

(2) Royall, C. P.; Vermolen, E. C. M.; van Blaaderen, A.; Tanaka, H. Controlling Competition between Crystallization and Glass Formation in Binary Colloids with an External Field. *J. Phys.: Condens. Matter* **2008**, *20*, 404225-1−404225-7.

(3) Frenkel, D. Colloidal Encounters: A Matter of Attraction. *Science* **2006**, *314*, 768−769.

(4) Anderson, V. J.; Lekkerkerker, H. N. W. Insights into Phase Transition Kinetics from Colloid Science. *Nature* **2002**, *416*, 811−815.

(5) Tikhonov, A.; Kornienko, N.; Zhang, J.; Wang, L.; Asher, S. Reflectivity Enhanced Two-Dimensional Dielectric Particle Array Monolayer Diffraction. *J Nanophotonics* **2012**, *6*, 063509-1−063509-9.

(6) Bohn, J.; Tikhonov, A.; Asher, S. Colloidal Crystal Growth Monitored by Bragg Diffraction Interference Fringes. *J. Colloid Interface Sci.* **2010**, *350*, 381−386.

(7) Weissman, J. M.; Sunkara, H. B.; Tse, A. S.; Asher, S. A. Thermally Switchable Periodicities from Novel Mesocopically Ordered Materials. *Science* **1996**, *274*, 959−960.

(8) Lee, K.; Asher, S. A. Photonic Crystal Chemical Sensors: pH and Ionic Strength. *J. Am. Chem. Soc.* **2000**, *122*, 9534−9537.

(9) Derjaguin, B. V.; Landau, L. Theory of the Stability of Strongly Charged Lyophobic Sols and of the Adhesion of Strongly Charged Particles in Solution of Electrolytes. *Acta Physicochim. URSS* **1941**, *14*, 633−662.

(10) Verwey, E.; Overbeek, J. *Theory of the Stability of Lyophobic Colloids*; Elsevier: New York, 1948.

(11) Alexander, S.; Chaikin, P. M.; Grant, P.; Morales, G. J.; Pincus, P.; Hone, D. Charge Renormalization, Osmotic Pressure, and Bulk Modulus of Colloidal Crystals: Theory. *J. Chem. Phys.* **1984**, *80*, 5776−5781.

(12) Trizac, E.; Bocquet, L.; Aubouy, M. Simple Approach for Charge Renormalization in Highly Charged Macroions. *Phys. Rev. Lett.* **2002**, *89*, 248301-1−248301-4.

(13) Aubouy, M.; Trizac, E.; Bocquet, L. Effective Charge Versus Bare Charge: An Analytical Estimate for Colloids in the Infinite Dilution Limit. *J. Phys. A: Math. Gen.* **2003**, *36*, 5835−5840.

(14) Trizac, E.; Bocquet, L.; Aubouy, M.; von Grünberg, H. H. Alexander's Prescription for Colloidal Charge Renormalization. *Langmuir* **2003**, *19*, 4027−4033.

(15) Hynninen, A. P.; Dijkstra, M. Phase Diagrams of Hard-Core Repulsive Yukawa Particles. *Phys. Rev. E* **2003**, *68*, 021407-1−021407-8.
(16) Egorov, S. A. Effect of Repulsive and Attractive Interactions on Depletion Forces in Colloidal Suspensions: A Density Functional Theory Treatment. *Phys. Rev. E* **2004**, *70*, 031402-1−031402-8.
(17) Sciortino, F.; Tartaglia, P. Glassy Colloidal Systems. *Adv. Phys.* **2005**, *54*, 471−524.
(18) Dawson, K.; Foffi, G.; Fuchs, M.; Götze, W.; Sciortino, F.; Sperl, M.; Tartaglia, P.; Voigtmann, T.; Zaccarelli, E. Higher-Order Glass-Transition Singularities in Colloidal Systems with Attractive Interactions. *Phys. Rev. E* **2000**, *63*, 011401-1−011401-17.
(19) Bussi, G.; Parrinello, M. Accurate Sampling Using Langevin Dynamics. *Phys. Rev. E* **2007**, *75*, 056707-1−056707-7.
(20) Bernal, J. Geometric Approach to the Structure of Liquids. *Nature* **1959**, *183*, 141−147.
(21) Aurenhammer, F. Voronoi Diagrams−A Survey of a Fundamental Geometric Data Structure. *ACM Comput. Surv.* **1991**, *23*, 345−405.
(22) Gilbert, E. N. Random Subdivisions of Space into Crystals. *Ann. Math. Stat.* **1962**, *33*, 958−972.
(23) Richards, F. The Interpretation of Protein Structures: Total Volume, Group Volume Distributions and Packing Density. *J. Mol. Biol.* **1974**, *82*, 1−14.
(24) Rycroft, C. H. VORO++: A Three-Dimensional Voronoi Cell Library in C++. *Chaos* **2009**, *19*, 041111−041111-1.
(25) Rycroft, C. H.; Grest, G. S.; Landry, J. W.; Bazan, M. Z. Analysis of Granular Flow in a Pebble-Bed Nuclear Reactor. *Phys. Rev. E* **2006**, *74*, 021306-1−021306-16.
(26) Libal, A.; Reichhardt, C.; Reichhardt, C. O. Point-Defect Dynamics in Two-Dimentional Colloidal Crystals. *Phys. Rev. E* **2007**, *75*, 011403-1−011403-7.
(27) Groh, B.; Mulder, B. A Closer Look at Crystallization of Parallel Hard Cubes. *J. Chem. Phys.* **2001**, *114*, 3653−3658.
(28) Marechal, M.; Zimmermann, U.; Löwen, H. Freezing of Parallel Hard Cubes with Rounded Edges. *J. Chem. Phys.* **2012**, *136*, 1−14.
(29) Smallenburg, F.; Filion, L.; Marechal, M.; Dijkstra, M. Vacancy-Stabilized Crystalline Order in Hard Cubes. *Proc. Natl. Acad. Sci. U.S.A.* **2012**, *109*, 17886−17890.
(30) Troadec, J. P.; Gervois, A.; Oger, L. Statistics of Voronoi Cells of Slightly Perturbed Face-Centered Cubic and Hexagonal Close-Packed Lattices. *Europhys. Lett.* **1998**, *42*, 167−172.
(31) Montoro, J. C. G.; Abascal, J. L. F. The Voronoi Polyhedra as Tools for Structure Determination in Simple Disordered Systems. *J. Phys. Chem.* **1993**, *97*, 4211−4215.
(32) Kumar, V. S.; Kumaran, V. Voronoi Neighbor Statistics of Hard-Disks and Hard-Spheres. *J. Chem. Phys.* **2005**, *123*, 074502-1−074502-10.
(33) Hamaguchi, S.; Farouki, R.; Dubin, D. Triple Point of Yukawa Systems. *Phys. Rev. E* **1997**, *56*, 4671−4682.
(34) Lindemann, F. The Calculation of Molecular Vibration Frequencies. *Phys. Z* **1910**, *11*, 609−612.
(35) Soma, T.; H.-Matsuo Kagaya, M. N. Mean-Square Displacement and Lindeman's Criterion for Melting of Alkali Metals. *Phys. Status Solidi B* **1983**, *115*, 273−276.